Numerical Simulation of Single-Phase and Multiphase Non-Darcy Flow in Porous and Fractured Reservoirs

Yu-Shu Wu
Earth Sciences Division
Lawrence Berkeley National Laboratory
Berkeley CA 94720, USA

Abstract

A numerical method as well as a theoretical study of non-Darcy fluid flow of through porous and fractured reservoirs is described. The non-Darcy flow is handled in a three-dimensional, multiphase flow reservoir simulator, while the model formulation incorporates the *Forchheimer* equation for describing single-phase or multiphase non-Darcy flow and displacement. The numerical scheme has been verified by comparing its results against those of analytical methods.

Numerical solutions are used to obtain some insight into the physics of non-Darcy flow and displacement in reservoirs. In addition, several type curves are provided for well-test analyses of non-Darcy flow to demonstrate a methodology for modeling this type of flow in porous and fractured rocks, including flow in geothermal reservoirs.

Key words: Non-Darcy flow, numerical reservoir simulation, well tests, multiphase flow, porous and fractured reservoirs.

1. Introduction

Darcy's law of flow (or Darcy flow), describing a linear relationship between volumetric flow rate (Darcy velocity) and pressure (head or potential) gradient, has been the fundamental principle in flow and transport processes in porous media (Muskat, 1946). Any deviations from this linear relation may be defined as non-Darcy flow. In this work our concern is only with the non-Darcy flow caused by high flow velocities. Even though Darcy's Law has been used nearly exclusively in the studies of porous-medium phenomena, there is considerable evidence that high-velocity non-Darcy flow occurs in many subsurface systems, such as in the flow near wells of oil or gas production, and liquid waste injection.

The effects of non-Darcy or high-velocity flow regimes in porous media have been observed and investigated for decades (e.g., Tek et al., 1962; Scheidegger, 1972; Katz and Lee, 1990). However, theoretical, field and experimental studies performed so far on non-Darcy flow in porous media have focused mostly on single-phase-flow conditions that pertain to the oil and gas industry (Tek et al., 1962; Swift and Kiel, 1962; Lee et al. 1987). Some investigations have been conducted for non-Darcy flow in fractured reservoirs (Skjetne et al., 1999) and for non-Darcy flow into highly permeable fractured wells (Guppy et al., 1981, 1982). Other studies have concentrated on finding and validating correlations of non-Darcy flow coefficients (Liu et al., 1995).

In the studies of non-Darcy flow through porous median, the *Forchheimer* equation is generally used

to describing single-phase non-Darcy flow. Several studies reported in the literature extend the *Forchheimer* equation to multiphase flow and provide equations for correlating non-Darcy flow coefficients under multiphase conditions (*Evans et al*., 1987; *Evans and Evans*, 1988; *Liu et al*., 1995). A recent study (*Wang* and *Mohanty*, 1999) has discussed the importance of multiphase non-Darcy flow in gas-condensate reservoirs and presents a pore-scale network model for describing non-Darcy gas-condensate flow. Because of insufficient study in this area as well as the mathematical difficulty in handling highly nonlinear, non-Darcy flow terms in multiphase flow equations, our understanding non-Darcy flow through porous media is very limited.

The objective of this study is to develop a numerical method for modeling single-phase and multiphase non-Darcy flow through heterogeneous porous and fractured rocks. The model formulation incorporates the *Forchheimer* equation, based on an integral finite-difference or a control volume numerical discretization scheme. The proposed model formulation is implemented into a three-dimensional, three-phase flow simulator and is applicable to both single-porosity porous media and fractured rocks. For flow in a fractured medium, fracture-matrix interactions are handled using a dual-continua approach, such as double- or multiple-porosity, or dual-permeability methods.

This paper discusses the model formulation and the numerical schemes implemented for modeling non-Darcy flow in porous media. The numerical scheme has been verified by comparing its results against those of analytical methods. As application examples, numerical solutions are used to obtain some insight into the physics of flow involving non-Darcy flow effects in reservoirs.

Furthermore, several type curves are provided for non-Darcy flow well-test analysis to demonstrate the proposed methodology for modeling this type of flow in porous and fractured rocks.

2. Governing Equations

A multiphase system in a porous or fractured aquifer is assumed to be composed of three phases: NAPL (oil), gas (air), and water. For simplicity, the three fluid components, water, NAPL, and gas, are assumed to be present only in their associated phases. Each phase flows in response to pressure, gravitational, and capillary forces according to the multiphase extension of Darcy's law for Darcy flow and the *Forchheimer* equation for non-Darcy flow. In an isothermal system containing three mass components, three mass-balance equations are needed to fully describe the system, as described in an arbitrary flow region of a porous or fractured domain:

For flow of phase f (f = w for water, f = n for NAPL or oil, and f = g for gas),

$$\frac{\partial}{\partial t}(\phi S_f \rho_f) = -\nabla \bullet (\rho_f \mathbf{v}_f) + q_f \qquad (2.1)$$

where ρ_f is the density of fluid f; $\mathbf{v}_f$ is the Darcy (or volumetric) velocity of fluid f; S_f is the saturation of fluid f; ϕ is the effective porosity of formation; t is time; and q_f is the sink/source term of phase (component) f per unit volume of formation.

Volumetric flow rate (namely Darcy velocity for Darcy flow) for non-Darcy flow of each fluid may be described using the multiphase extension of *Forchheimer* equation (Evans and Evans, 1988; Liu et al., 1995):

$$-\left(\nabla P_f - \rho_f \mathbf{g}\right) = \frac{\mu_f}{k k_{rf}} \mathbf{v}_f + \beta_f \rho_f \mathbf{v}_f \left|\mathbf{v}_f\right| \qquad (2.2)$$

where P_f is the pressure of phase f; $\mathbf{g}$ is the gravitational constant vector; k is the absolute/intrinsic permeability (tensor) of the formation; k_{rf} is relative permeability to phase f; and β_f is the effective non-Darcy flow coefficient with a unit m^{-1} for fluid f under multiphase flow conditions (Evans and Evans, 1988).

Under single-phase flow conditions the coefficient, β_f, is traditionally called a turbulence coefficient or an inertial resistance coefficient (Tek et al., 1962; Lee et al. 1987). Note that to include multiphase effects on non-Darcy flow, Equation (2.2) is modified by the following:

- Pressure gradient is replaced by flow potential gradient [the left-hand-side term of (2.2)] to include gravity effects.
- Absolute permeability is replaced by an effective permeability term ($k k_{rf}$).
- β_f is described as the effective non-Darcy flow coefficient for a flowing phase under multiphase flow conditions.

Darcy law's states that a linear relationship exists between volumetric flow rate and pressure (head or potential) gradient in porous media. The linear term, the first term $\left(\frac{\mu_f}{k k_{rf}} \mathbf{v}_f\right)$ on the right-hand side of Equation (2.2), represents viscous flow; it is dominant at low flow rates. Additional pressure drop or energy assumption resulting from non-Darcy or high flow velocities is described by the second term

$\left(\beta_f \rho_f \mathbf{v}_f |\mathbf{v}_f|\right)$ on the right-hand side of (2.2) for the extra friction or inertial effects (*Katz and Lee*, 1990).

Equation (2.2) indicates that the non-Darcy flow equation reduces to the multiphase Darcy law

If the non-Darcy term $\left(\beta_f \rho_f \mathbf{v}_f |\mathbf{v}_f|\right)$ can be ignored, when compared with the first term $\left(\frac{\mu_f}{k k_{rf}} \mathbf{v}_f\right)$,

for low flow velocity, Equation (2.2) becomes a Darcy's law. For high velocities, however, the second term becomes dominant and must be included. Therefore, Darcy flow can generally be considered as a special case of non-Darcy flow as described by Equation (2.2.).

Equation (2.2) implicitly defines the Darcy velocity as a function of pressure gradient as well as saturation and relative permeability. A more general relation for the Darcy velocity in multiphase non-Darcy flow may be proposed as a function of pressure gradient, saturation, and relative permeability functions:

$$\mathbf{v}_f = \mathbf{v}_f\left(\nabla P_f, S_f, k_{rf}\right) \tag{2.3}$$

With Equation (2.3), many other kinds of equations for non-Darcy flow in addition to the *Forchheimer* equation (e.g., Scheidegger, 1972) can be extended to multiphase non-Darcy flow situations.

Equation (2.1), the governing of mass balance for three phases, needs to be supplemented with constitutive equations, which express all the secondary variables and parameters as functions of a set

of primary thermodynamic variables of interest. The following relationships will be used to complete the description of multiphase flow through porous media:

$$S_w + S_n + S_g = 1 \tag{2.4}$$

The capillary pressures relate pressures between the phases. The aqueous- and gas-phase pressures are related by

$$P_w = P_g - P_{cgw}\left(S_w\right), \tag{2.5}$$

where P_{cgw} is the gas-water capillary pressure in a three-phase system and assumed to be a function of water saturation only. The NAPL pressure is related to the gas phase pressure by

$$P_n = P_g - P_{cgn}\left(S_w,\ S_n\right), \tag{2.6}$$

where P_{cgn} is the gas-NAPL capillary pressure in a three-phase system, which is a function of both water and NAPL saturations. For many aquifer formations, the wettability order is (1) aqueous phase, (2) NAPL phase, and (3) gas phase. The gas-water capillary pressure is usually stronger than the gas-NAPL capillary pressure. In a three-phase system, the NAPL-water capillary pressure, P_{cnw}, may be defined as

$$P_{cnw} = P_{cgw} - P_{cgn} = P_n - P_w \tag{2.7}$$

The relative permeabilities are assumed to be functions of fluid saturations only. The relative permeability to the water phase is described by

$$k_{rw} = k_{rw}\left(S_w\right) \tag{2.8}$$

to the NAPL phase by

$$k_{rn} = k_{rn}\left(S_w, S_g\right) \tag{2.9}$$

and to the gas phase by

$$k_{rg} = k_{rg}\left(S_g\right) \tag{2.10}$$

The densities of water, NAPL, and gas, as well as the viscosities of fluids, can in general be treated as functions of fluid pressures.

3. Numerical Formulation

The multiphase non-Darcy flow equations, as discussed in Section 2, have been implemented into a general-purpose, three-phase reservoir simulator, the MSFLOW code [Wu, 1998]. As implemented in the code, Equation (2.1) can be discretized in space using an integral finite-difference or control-volume finite-element scheme for a porous and/or fractured medium. The time discretization is carried out with a backward, first-order, finite-difference scheme. The discrete nonlinear equations for water, NAPL, and gas flow at Node i are written as follows:

$$\left\{\left(\phi\, S_f \rho_f\right)_i^{n+1} - \left(\phi\, S_f \rho_f\right)_i^{n}\right\}\frac{V_i}{\Delta t} = \sum_{j\in\eta_i}\left(F_f\right)_{ij}^{n+1} + Q_{fi}^{n+1} \tag{3.1}$$

where n denotes the previous time level; n+1 is the current time level; V_i is the volume of element i (porous or fractured block); Δt is the time step size; η_i contains the set of neighboring elements (j), porous or fractured block, to which element i is directly connected; and F_f is a mass flow term between elements i and j, defined [when Equation (2.2) is used] as

$$F_f = \frac{A_{ij}}{2(k\beta_f)_{ij+1/2}}\left\{-\frac{1}{\lambda_f}+\left[\left(\frac{1}{\lambda_f}\right)^2-\gamma_{ij}\left(\psi_{fj}-\psi_{fi}\right)\right]^{1/2}\right\} \tag{3.2}$$

where subscript ij+1/2 denotes a proper averaging of properties at the interface between the two elements and A_{ij} is the common interface area between connected elements i and j. The mobility of phase f is defined as

$$\lambda_f = \frac{k_{rf}}{\mu_f} \tag{3.3}$$

and the flow potential term is

$$\psi_{fi} = P_{fi} - \rho_{ij+1/2} g D_i \tag{3.4}$$

where D_i is the depth to the center of element i. The mass sink/source term at element i, Q_{fi} for phase f, is defined as

$$Q_{fi} = q_{fi} V_i \tag{3.5}$$

In (3.2), transmissivity of flow terms is defined (if the integral finite-difference scheme is used) as,

$$\gamma_{ij} = \frac{4(k^2 \rho_f \beta_f)_{ij+1/2}}{d_i + d_j}, \tag{3.6}$$

where d_i is the distance from the center of element i to the interface between elements i and j.

In the model formulation, absolute permeability, relative permeability and effective non-Darcy flow coefficient are all considered as flow properties of porous media and need to be averaged between connected elements in calculating the mass flow terms. In general, weighting approaches used are

that absolute permeability is harmonically weighted along the connection between elements i and j, relative permeability and non-Darcy flow coefficients are both upstream weighted.

Newton/Raphson iterations are used to solve Equation (3.1). For a three-phase flow system, $3 \times N$ coupled nonlinear equations must be solved (N being the total number of elements of the grid), including three equations at each element for the three mass-balance equations of water, NAPL, and gas, respectively. The three primary variables (x_1, x_2, x_3) selected for each element are gas pressure, gas saturation, and NAPL saturation, respectively. In terms of the three primary variables, the Newton/Raphson scheme gives rise to

$$\sum_m \frac{\partial R_i^{\beta, n+1}\left(x_{m,p}\right)}{\partial x_m}\left(\delta x_{m,p+1}\right) = -R_i^{\beta,n+1}\left(x_{m,p}\right) \qquad \text{for m = 1, 2, and 3} \tag{3.7}$$

where index m = 1, 2, and 3 indicates the primary variable 1, 2, or 3, respectively; p is the iteration level; and i = 1, 2, 3, …, N, the nodal index. The primary variables are updated after each iteration:

$$x_{m,p+1} = x_{m,p} + \delta x_{m,p+1} \tag{3.8}$$

A numerical method is used to construct the Jacobian matrix for Equation (3.7), as outlined by Forsyth et al. (1995).

4. Treatment of Boundary Conditions and Fractured Media

First-type or Dirichlet boundary conditions denote constant or time-dependent phase pressure, and saturation conditions. These types of boundary conditions can be treated using the large-volume or inactive-node method (Pruess, 1991), in which a constant pressure/saturation node may be specified with a huge volume while keeping all the other geometric properties of the

mesh unchanged. However, caution should be taken in (1) identifying phase conditions when specifying the "initial condition" for the large-volume boundary node and (2) distinguishing upstream/injection from downstream/production nodes. Once specified, primary variables will be fixed at the big-volume boundary nodes, and the code handles these boundary nodes exactly like any other computational nodes.

Flux-type or Neuman boundary conditions are treated as sink/source terms, depending on the pumping (production) or injection condition, which can be directly added to Equation (3.1). This treatment of flux-type boundary conditions is especially useful for a situation where flux distribution along the boundary is known, such as dealing with a single-node well. More general treatment of multilayered well-boundary conditions is discussed in Wu (2000a).

The technique used in the current model for handling flow and transport through fractured rock follows the dual-continuum methodology (Warren and Root, 1963; Pruess, 1991; Pruess and Narasimhan, 1985). The method treats fracture and rock matrix flow and interactions using a multi-continuum numerical approach, including the double- or multiporosity method (Wu and Pruess, 1988), the dual-permeability method, and the more general "multiple interacting continua" (MINC) method (Pruess and Narasimhan, 1985).

The model formulation involved in modeling non-Darcy flow is applicable to both single-continuum and multi-continuum media. When handling flow through a fractured rock, the problem becomes essentially how to generate a mesh that represents both the fracture and matrix systems. Several fracture-matrix subgridding schemes exist for designing different meshes for different fracture-matrix conceptual models (*Pruess*, 1983). Once a proper mesh of a fracture-matrix system is generated, fracture and matrix blocks are specified to represent fracture or matrix domains, separately. Formally, they are treated exactly the same in the solution by the model. However, physically consistent fracture and matrix properties and modeling conditions must be appropriately specified for fracture and matrix systems, respectively.

5. Model Verification Examples

In this section we provide three examples to verify the proposed numerical schemes involved in handling non-Darcy flow of single-phase and multi-phase fluids in porous and fractured media. Several analytical solutions are used in these comparisons. The sample problems include:

- Single-phase, steady-state non-Darcy flow in homogenous porous media
- Single-phase, transient flow through a double-porosity reservoir
- Two-phase non-Darcy flow and displacement in homogenous porous media

5.1 Single-Phase, Steady-State Radial Flow

This problem is used to verify the numerical scheme for modeling steady-state, non-Darcy flow in homogeneous porous media. For the comparative study, an exact analytical solution for this problem is presented in Appendix A. The test problem concerns steady-state, one-dimensional, and horizontal radial flow toward a well in a uniform and homogeneous system. A non-Darcy flow correlation from Tek et al. (1962) is used to evaluate the non-Darcy flow coefficient β versus porosity and permeability as follows:

$$\beta = \frac{C_\beta}{k^{5/4}\phi^{3/4}} \tag{5.1}$$

where C_β is a non-Darcy flow constant with a unit ($m^{3/2}$) when converted to S.I. units.

The numerical solution of this problem is performed by the multiphase flow code, MSFLOW, in which single-phase flow is handled as a special case of three-phase flow. A one-dimensional,

radial-symmetric grid of 2,200 elements was generated along the 1,000 meters of the radial flow direction. The parameters used for the comparison are listed in Table 5.1 for evaluating both analytical and numerical solutions. Comparisons of pressure distributions along the radial direction, calculated from the exact and numerical solutions, are shown in Figure 5.1. The agreement between the two solutions is excellent for different non-Darcy flow coefficients. In fact, many additional steady-state simulations have been performed and the numerical results are found to be in excellent agreement with the analytical solution in every case.

5.2 Single-Phase Fractured-Medium Flow Problem

This problem tests the numerical formulation for simulating transient flow in fractured media by comparison with an analytical solution. The example concerns transient flow towards a well that fully penetrates a horizontal, uniform, fractured, radially infinite reservoir. When non-Darcy flow effects are small or can be ignored, the analytical solution by Warren and Root (1963) can be used for this particular test.

A radially symmetrical reservoir ($r = 5 \times 10^6$ m) is discretized into a one-dimensional (r), primary grid. The r-distance of 5×10^6 meters is subdivided into 3,100 intervals in logarithmic scale. A double-porosity mesh is generated from the primary grid, in which a three-dimensional fracture network and cubic matrix blocks are used. The matrix block size is $1 \times 1 \times 1$ meter, and fracture permeability and aperture are correlated by the cubic law. Input parameters are given in Table 5.2. Note that 10-times-larger non-Darcy flow coefficients than those for fractures are used

correspondingly for flow in matrix to account for lower matrix permeability. A fully penetrating pumping well is represented by a well element with a specified constant water-pumping rate.

Figure 5.2 shows a comparison of the numerical modeling results and the Warren and Root solution for the pressure response at the well, in which the dimensionless variables were defined by Warren and Root (1963). Figure 5.2 shows that the simulated pressures at the well are in excellent agreement with the analytical solution, with a typical double-porosity behavior of two-parallel semi-log straight lines developed on the plot.

5.3 Two-Phase Non-Darcy Displacement

In this problem, an analytical solution (Wu, 2000b) is used to examine the validity of the numerical method for modeling multiphase non-Darcy flow and displacement processes. The *Forchheimer* equation is also used for the comparison. The physical flow model is a one-dimensional linear porous medium, which is at first saturated uniformly with a nonwetting fluid ($S_n = 0.8$) and a wetting fluid ($S_w = S_{wr} = 0.2$). A constant volumetric injection rate of the wetting fluid is imposed at the inlet ($x = 0$), starting from $t = 0$. The relative permeability curves used for all the calculations in this problem are shown in Figure 5.3, and rock and fluid properties are listed in Table 5.3.

In this problem, the effective non-Darcy flow coefficient for multiphase flow is treated as a function of fluid saturation and relative permeability. The non-Darcy flow coefficient correlation, defined by Equation (5.1), is extended to the two-phase flow situation with replacing the absolute permeability

(k) by an effective permeability (k k_{rf}) and replacing porosity ϕ with $\phi(S_f - S_{fr})$. Then, we can derive the relationship for the non-Darcy flow coefficient as follows:

$$\beta_f(S_w, k_{rf}) = \frac{C_\beta}{(k k_{rf})^{5/4}\left[\phi(S_f - S_{fr})\right]^{3/4}} \tag{5.2}$$

where S_{fr} is residual saturation of fluid f. Equation (5.2) is incorporated into both the analytical and numerical calculations.

To reduce the effects of discretization on numerical simulation results, we choose very fine, uniform mesh spacing (Δx = 0.01 m). A one-dimensional 5 m linear domain is discretized into 500 one-dimensional uniform gridblocks. In the numerical simulation, the non-Darcy flow coefficient, Equation (5.2), is treated as a flow property and is evaluated using a full upstream weighting scheme such as that for the relative permeability function.

Figure 5.4 shows saturation profiles after 10 hours from both analytical and numerical solutions. The figure indicates that the numerical results are in excellent agreement with the analytical prediction of the non-Darcy displacement for the entire wetting-phase sweeping zone. Except at the shock, advancing saturation front, the numerical solution deviates only slightly from the analytical solution, resulting from a typical "smearing front" phenomenon of numerical dispersion effects that occurs when matching the Buckley-Leverett solution using numerical results (Aziz and Settari, 1979).

6. Application and Discussion

In this section, we present several application examples and discuss single-phase, non-Darcy flow behavior to demonstrate the applicability of the present modeling approach to field problems. The application examples generate dimensionless pressures or type curves for non-Darcy flow well test analyses, including:

(1) Pressure drawdown and buildup analyses
(2) Effects of finite boundaries of reservoirs
(3) Pressure drawdown in fractured reservoirs
(4) Well test determination of non-Darcy flow coefficients

Before further discussing these application problems, we introduce several dimensionless variables for analyzing single-phase flow and well test results (Earlougher, 1977). Let us define the following group of dimensionless variables:

The dimensionless radius,

$$r_D = \frac{r}{r_w} \tag{6.1}$$

the dimensionless time,

$$t_D = \frac{kt}{\phi_i \mu C_t r_w^2} \tag{6.2}$$

the dimensionless non-Darcy flow coefficient,

$$\beta_D = \frac{k q_m \beta}{2\pi r_w h \mu} \tag{6.3}$$

and the dimensionless pressure,

$$P_D = \frac{P_i - P}{\frac{q_v \mu}{2\pi kh}} \tag{6.4}$$

In these notations, the subscript referring to a phase is ignored, r is radial distance (coordinate), r_w is wellbore radius, ϕ_i is the effective (or initial) porosity of formation at reference (initial)

pressure ($P = P_i$), C_t is total compressibility of fluid and rock, h is thickness of formation, q_m is mass production or injection rate, and q_v is volumetric production or injection rate.

6.1 Pressure Drawdown and Buildup Analyses

This example presents a set of type curves for analyzing well tests of single-phase, slightly compressible non-Darcy fluid flow in an infinite-acting reservoir. The basic modeling parameters are summarized in Table 6.1. Non-Darcy flow is considered to occur into a fully penetrating well from an infinite-acting, homogeneous and isotropic, uniform and horizontal formation. Even though skin and wellbore storage effects are ignored in the results, they can easily be included if needed.

The infinite-acting reservoir is approximated by a one-dimensional, radially symmetrical reservoir in the numerical model with age outer boundary radius of 5×10^6 (m), discretized into a one-dimensional grid of 3,100 gridblocks in logarithmic scale. Initially, the system is undisturbed and at constant pressure. A fully penetrating injection well, represented by a well element, starts pumping at $t = 0$, specified at a constant water-pumping rate.

A set of type-curves for pressure drawdown, calculated by the numerical model in terms of dimensionless pressure versus dimensionless time, is shown in Figure 6.1. Figure 6.1 clearly indicates that the non-Darcy flow coefficient is a very important and sensitive parameter to the pressure drawdown curves. When non-Darcy flow coefficients are sufficiently large, they affect pressure transient behavior during both earlier and later times. Note that in the simulation, the non-Darcy flow coefficient is evaluated to be uncorrelated with other parameters. Figure 6.1 indicates that the non-Darcy flow coefficient can be effectively estimated using the type curves with the traditional type-curve matching approach. Note also that for small non-Darcy flow coefficients, pressure declines at the well

during pumping are approaching those predicted by Theis solution, as it should be. This results from the diminishing effect of non-Darcy flow with flow behavior now tending towards to Darcy flow regime.

Figure 6.2 presents simulated pressure drawdown and buildup curves, in which the well is pumped for one day only and then shut off. The well pressure variations during the entire pumping and shut-in period, as shown in Figure 6.2, indicate that pressure buildup is insensitive to the values of non-Darcy flow coefficients, as compared with drawdown in pumping periods. This is because of rapid reduction in flow velocity near the well after a well is shut off and non-Darcy flow effects become ineligible. Many additional modeling investigations have verified this observation has been confirmed. This indicates that pressure-buildup tests are not suitable for estimating non-Darcy flow coefficients. On the other hand, the pressure-buildup method, following non-Darcy flow pumping tests, will be a good test for determining permeability values without significant non-Darcy flow.

6.2 Effects of Finite Reservoir Boundaries

For practical well tests, boundary effects or well interferences in finite, developed reservoirs will show up sooner or later. Two types of boundary conditions, closed and constant pressure conditions, are commonly used to approximate the effects of finite reservoir/well boundaries. In this section, effects of finite-system boundary conditions on pressure drawdown behavior will be discussed.

The flow system and parameters for finite systems are similar to those in Section 6.1. Only two finite radial systems with outer boundary radii (r_e =1,000 and 10,000 m) are considered. Figures

6.3 and 6.4 show dimensionless pressure drawdown curves, for closed and constant-pressure boundaries as well as the two radii. For a smaller formation system with r_e = 1,000 m, Figure 6.3 shows that significant boundary effects occur at about dimensionless time $t_D = 10^8$ (1 day in real time), at which the well pressure responses deviate from the infinite-acting solution (say, the Theis solution for small non-Darcy flow coefficients). For the larger system with r_e = 10,000 m, boundary effects are very similar but show up much later (Figure 6.4).

6.3 Analysis of non-Darcy Flow in Fractured Media

This problem portrays non-Darcy flow through a fractured reservoir. The fracture-matrix formation is described using the Warren and Root double-porosity model. The physical flow model is the same as that in Section 5.2 for one-dimensional fracture-matrix system, with basic properties of rock and fluid also given in Table 5.2.

For non-Darcy flow into a well from an infinite fractured system, well pressures type curves are shown in semi-log plots of Figure 6.5. The type curves on the figures show that well (fracture) pressures are extremely sensitive to the value of non-Darcy flow coefficients; therefore, well pumping tests will help determine this constant in a fractured reservoir. Furthermore, Figure 6.5 indicates that the effects of non-Darcy flow on early transient pressure responses are very strong, such that the first semi-log straight lines may not develop when non-Darcy flow is involved.

6.4 Determination of Non-Darcy Flow Coefficients

In addition to the type-curve matching method for determining non-Darcy flow coefficients (as discussed above), we may derive a simpler approach. Type-curves observation in Figures 6.1 - 6.5 indicates that vertical displacement (difference in dimensionless pressures) at the same time between non-Darcy and Darcy flow solutions is always closely related to (dimensionless) non-Darcy flow coefficients as long as closed boundary effects are insignificant. A close examination of Figure 6.1 or 6.5 reveals:

$$\Delta P_D \approx \beta_D \tag{6.5}$$

after the early transient times ($t_D = 10^5$ or 1,000 seconds in real time). Is this true? This can be further illustrated using a simple steady-state solution, provided in Appendix A. At steady-state and if $r_e >> r_w$, the solution (A.15) becomes

$$P_D = \ln\left(\frac{r_D^e}{r_D}\right) + \beta_D\left(\frac{1}{r_D} - \frac{1}{r_D^e}\right) \approx \ln\left(r_D^e\right) + \beta_D \tag{6.6}$$

at wells with $r = r_w$ or $r_D = 1$. The first term of (6.6), on the right-hand side, is identical to the solution for steady-state Darcy flow. Therefore, the difference in dimensionless pressure under steady state is approximately equal to a dimensionless non-Darcy flow coefficient, as defined in Equation (6.3). It is encouraging to note that this relation may provide a good approximation even for unsteady-state flow conditions after earlier transient periods, as shown in Figures 6.1 - 6.5.

The correlation of dimensionless non-Darcy flow coefficients with dimensionless pressures, as shown in Figure 6.1 and 6.5, as well as Equation (6.6), is equivalent to that of skin effects in a Darcy flow well-test analysis (Earlougher, 1977). This indicates that the non-Darcy flow effect is dominated mainly by the flow near the wellbore, because of the much higher flow velocities

there. In general, skin and non-Darcy flow effects cannot be separated from a single well test under non-Darcy flow condition. We recommend that skin effects be estimated using a low flow rate or Darcy flow test first.

Here, an example demonstrates how to use Equation (6.5) to determine non-Darcy flow coefficients by well tests. This simple method can be demonstrated using the simulated well test of Section 6.1. From the simulation, at $t_D = 0.1243 \times 10^8$ (or $t = 0.3778 \times 10^5$ sec.) the dimensionless well pressure $P_D = 18.53$ for $\beta_D = 10$, and $P_D = 8.52$ for $\beta_D = 0$. Substituting these dimensionless pressure difference data into Equation (5.6), together with the definition (6.3),

$$\beta = \frac{\beta_D (2\pi r_w h\mu)}{k q_m} \approx \frac{\Delta p_D (2\pi r_w h\mu)}{k q_m} = \frac{(18.53 - 8.52) \times 2 \times \pi \times 10 \times 10^{-3}}{9.869 \times 10^{-13} \times 0.1} = 6.36 \times 10^{12} (m^{-1}) \qquad (6.3)$$

The actual input value for β is 6.37×10^{12} in for the numerical test problem. The result indicates that the proposed well test method is very accurate for determining non-Darcy flow coefficients in this case.

7. Summary and Conclusions

This paper presents a numerical method and theoretical study for non-Darcy flow and displacement through porous and fractured media. A three-dimensional, three-phase flow reservoir simulator has been enhanced to include the capability of modeling non-Darcy flow. Model formulation incorporates the *Forchheimer* equation to describe single-phase and multiphase non-Darcy flow. The numerical scheme implemented has been verified by comparing numerical simulation results

with those of analytical solutions under single-phase and multiphase, steady-state and transient flow conditions. As application examples, numerical solutions are used to obtain some insight into the physics of flow involving non-Darcy flow effects in porous media. It has been found that pressure drawdown not buildup behavior is sensitive to effects of non-Darcy flow, therefore pressure drawdown testing will be a suitable approach for well-testing determination of non-Darcy flow coefficients. In addition, several type curves and a simplified method are provided for well test analyses of non-Darcy flow to demonstrate the proposed methodology's usefulness for investigating non-Darcy flow in porous and fractured rocks.

Acknowledgement

The author is indebted Jianchun Liu and Dan Hawkes for their careful and critical review of this manuscript. This work was supported in part by the Assistant Secretary for Energy Efficiency and Renewable Energy, Office of Geothermal and Wind Technologies of the U.S. Department of Energy, under Contract No. DE-AC03-76SF00098.

References

Aziz, K. and A. Settari, *Petroleum Reservoir Simulation,* Applied Science, London, 1979.

Earlougher, R. C. Jr., *Advances in Well Test Analysis*, SPE Monograph, Vol. 5, SPE of AIME, Dallas, 1977.

Evans, E. V. and R. D. Evans, Influence of an immobile or mobile saturation on non-Darcy compressible flow of real gases in propped fractures, *J. Petroleum Technology,* Vol. 40, No. 10, 1343-1351, 1988.

Evans, R. D., C. S. Hudson and J. E. Greenlee, The effect of an immobile liquid saturation on the non-Darcy flow coefficient in porous media, *J. SPE Production Engineering, Trans*. AIME, Vol. 283, 331-338, 1987.

Forsyth, P. A., Y. S. Wu and K. Pruess, Robust numerical methods for saturated-unsaturated flow with dry initial conditions in heterogeneous media, *Advances in Water Resources,* Vol. 18, pp. 25-38, 1995.

Guppy, K. H., H. Cinco-Ley, H. J. Ramey, Jr. and F. Samaniego, Non-Darcy flow in wells with finite-conductivity vertical fractures, *Soc. Pet. Eng. J.,* 681-698, 1982.

Guppy, K. H., H. Cinco-Ley, and H. J. Ramey, Jr., Effects of non-Darcy flow on the constant-pressure production of fractured wells, *Soc. Pet. Eng. J.,* 390-400, 1981.

Katz, D. L. and R. L. Lee, *Natural Gas Engineering, Production and Storage*, Chemical Engineering Series, McGraw-Hill Book Co. Inc., New York, 1990.

Lee, R. L., R. W. Logan and M. R. Tek: "Effetcs of turbulence on transient flow of real gas through porous media," *SPE Formation Evaluation*, 108-120, 1987.

Liu, X., F. Civan and R. D. Evans, Correlations of the non-Darcy flow coefficient, *J. Canadian Petroleum Technology,* Vol. 34, No. 10, 50-54, 1995.

Muskat, M., *The Flow of Homogeneous Fluids through Porous Media*, J. W. Edwards, Inc., Ann Arbor, Michigan, 1946.

Pruess, K., TOUGH2 - A General-Purpose Numerical simulator for multiphase fluid and heat flow, Report LBL-29400, Lawrence Berkeley National Laboratory, Berkeley, California, 1991.

Pruess, K. and Narasimhan, T. N., A practical method for modeling fluid and heat flow in fractured porous media, *Soc. Pet. Eng. J., 25,* pp. 14-26, 1985.

Pruess, K., GMINC - A mesh generator for flow simulations in fractured reservoirs, Report LBL-15227, Berkeley, California: Lawrence Berkeley National Laboratory, 1983.

Scheidegger, A. E. *The Physics of Flow through Porous Media,* University of Toronto Press, 1972.

Skjetne, E., T. K. Statoil and J. S. Gudmundsson, Experiments and modeling of high-velocity pressure loss in sandstone fractures, SPE 56414, Presented at the 1999 SPE Annual Technical Conference and Exhibition, Houston, Texas, 3-6, October, 1999.

Swift, G. W. and O. G. Kiel, The prediction of gas-well performance including the effects of non-Darcy flow, *J. Petroleum Technology, Trans*. AIME, Vol. 222, 791-798, 1962.

Tek, M. R., K. H. Coats and D. L. Katz, The effects of turbulence on flow of natural gas through porous reservoirs, *J. Petroleum Technology, Tran.s* AIME, Vol. 222, 799-806, 1962.

Wang, X. and K. K. Mohanty, Multiphase non-Darcy flow in gas-condensate reservoirs, SPE 56486, Presented at the 1999 SPE Annual Technical Conference and Exhibition, Houston, Texas, 3-6, October, 1999.

Warren, J.E., and P. J. Root, The behavior of naturally fractured reservoirs, *Soc. Pet. Eng. J., Trans., AIME*, pp. 245-255, 228, 1963.

Wu, Y. S. "A virtual node method for handling wellbore boundary conditions in modeling multiphase flow in porous and fractured media," LBNL-42882, Vol. 36, N0. 3, pp.807-814, ***Water Resources Research***, March, 2000a.

Wu, Y. S. "Non-Darcy displacement of immiscible fluids in porous media," LBNL-45228, Lawrence Berkeley National Laboratory, Berkeley, California, 2000b.

Wu, Y. S., MSFLOW: *Multiphase Subsurface Flow Model of Oil, Gas and Water in Porous and Fractured Media with Water Shut-off Capability*, *DOCUMENTATION and User's Guide*, Walnut Creek, California, 1998.

Wu, Y. S. and K. Pruess, A multiple-porosity method for simulation of naturally fractured petroleum reservoirs, *SPE Reservoir Engineering*, 3, pp. 327-336, 1988.

Table 5.1 Parameters for the steady-state single-phase flow problem.

Parameter	Value	Unit
Reference Pressure	$P_i = 10$	Bar
Reference Porosity	$\phi_i = 0.20$	
Reference Fluid Density	$\rho_i = 1{,}000$	kg/m^3
Formation Thickness	h=10	m
Fluid Viscosity	$\mu = 1\times10^{-3}$	Pa•s
Fluid Compressibility	$C_f=5 \times 10^{-10}$	Pa^{-1}
Rock Compressibility	$C_r=5 \times 10^{-9}$	Pa^{-1}
Permeability	$k = 9.869\times10^{-13}$	m^2
Water Production Rate	$q_m = 0.1$	kg/s
Wellbore Radius	$r_w = 0.1$	m
Outer Boundary Radius	r_e=1,000	m
non-Darcy flow constant	$C_\beta = 3.2 \times 10^{-3}$, 3.2×10^{-4}, 3.2×10^{-9}	$m^{3/2}$

Table 5.2 Parameters for the single-phase, fractured-medium flow problem.

Parameter	Value	Unit
Matrix Porosity	$\phi_M = 0.30$	
Fracture Porosity	$\phi_F = 0.0006$	
Reference Water Density	$\rho_w = 1{,}000$	kg/m^3
Water Phase Viscosity	$\mu_w = 1 \times 10^{-3}$	Pa•s
Matrix Permeability	$k_M = 1.0 \times 10^{-16}$	m^2
Fracture Permeability	$k_F = 9.869 \times 10^{-13}$	m^2
Water Production Rate	$q_m = 0.1$	kg/s
Rock Compressibility	$C_r = 1.0 \times 10^{-9}$	1/Pa
Water Compressibility	$C_w = 5.0 \times 10^{-10}$	1/Pa
Dimensionless non-Darcy Flow Coefficient for fracture	$\beta_{D,f} = 1 \times 10^{-4}$, 1, 5, and 10	
Dimensionless non-Darcy Flow Coefficient for matrix	$\beta_{D,m} = 1 \times 10^{-3}$, 10, 50, and 100	
Wellbore Radius	$r_w = 0.1$	m

Table 5.3 Parameters for the non-Darcy Displacement Example.

Parameter	Value	Unit
Effective Porosity	$\phi = 0.30$	
Permeability	$k = 9.869 \times 10^{-13}$	m^2
Wetting Phase Density	$\rho_w = 1{,}000$	kg/m^3
Wetting Phase Viscosity	$\mu_w = 1.0 \times 10^{-3}$	Pa•s
Nonwetting Phase Density	$\rho_n = 800$	kg/m^3
Nonwetting Phase Viscosity	$\mu_n = 5.0 \times 10^{-3}$	Pa•s
non-Darcy Flow Constant	$C_\beta = 3.2 \times 10^{-6}$	$m^{3/2}$
Injection Rate	$q_v = 1.0 \times 10^{-5}$	m^3/s

Table 6.1 Parameters for the pressure drawdown and buildup analysis.

Parameter	Value	Unit
Initial Pressure	$P_i = 10$	Bar
Initial Porosity	$\phi_i = 0.20$	
Reference Fluid Density	$\rho_i = 1{,}000$	kg/m^3
Formation Thickness	$h=10$	m
Fluid Viscosity	$\mu = 1\times10^{-3}$	Pa•s
Fluid Compressibility	$C_f=5 \times 10^{-10}$	Pa^{-1}
Rock Compressibility	$C_r=5 \times 10^{-9}$	Pa^{-1}
Permeability	$k = 9.869\times10^{-13}$	m^2
Water Injection Rate	$q_v = 0.1$	m^3/d
Wellbore Radius	$r_w = 0.1$	m
Outer Boundary Radius	$r_e= \infty \approx 5\times 10^6$	m
Dimensionless non-Darcy Flow Coefficient	$\beta_D = 1 \times 10^{-3}$, 1, 10, 100 1×10^3, 1×10^4, 1×10^5	

Nomenclature

C_f fluid compressibility (Pa^{-1})

C_r rock (porosity) compressibility (Pa^{-1})

C_t total compressibility (Pa^{-1})

C_β non-Darcy flow constant ($m^{3/2}$)

d_i distance to the interface from gridblock i a (m)

D_i depth to the center of gridblock i (m)

F_f mass flux of fluid f (kg/s)

g, **g** gravitational constant (m/s^2)

h thickness of formation (m)

k absolute permeability (m^2)

k_F fracture permeability (m^2)

k_M matrix permeability (m^2)

k_{rf} relative permeability to phase f

P pressure (Pa)

P_{cgn} gas-NAPL capillary pressure (Pa)

P_{cgw} gas-water capillary pressure (Pa)

P_{cnw} NAPL-water capillary pressure (Pa)

P_D dimensionless pressure (Pa)

P_g gas pressure (Pa)

P_n NAPL pressure (Pa)

P_w water pressure (Pa)

Q_f mass sink/source term (kg/s)

R^f mass residual term (kg/s)

q_f mass sink/source term (kg/s m^3)

q_m mass injection rate (kg/s)

q_v volumetric injection rate (m^3/s)

S_g gas pressure (Pa)

S_n NAPL pressure (Pa)

S_w water pressure (Pa)

x_m primary variables to residual equations

r radial distance (m)

r_D dimensionless radius

r_e outer boundary radius (m)

r_w wellbore radius (m)

t time (s)

t_D dimensionless time, Equation (42)

v Darcy or volumetric flow velocity (m/s)

v_r radial Darcy or volumetric flow rate (m/s)

V_i volume of gridblock i (m^3)

β, β_f non-Darcy flow coefficient of fluid f (m^{-1})

γ_{ij} transmissivity between gridblocks i and j (kg/ m^3)

λ_f mobility of fluid f $(Pa \bullet s)^{-1}$

μ, μ_f viscosity of fluid f (Pa•s)

ρ_f density of fluid f (kg/m^3)

ρ_i initial or reference fluid density (kg/m^3)

ϕ porosity

ϕ_i initial or reference porosity

ψ_f flow potential term (Pa)

Figure Captions

Figure 5.1 Comparison of dimensionless pressures calculated from exact and numerical solutions for steady-state non-Darcy flow with different non-Darcy flow coefficients.

Figure 5.2 Comparison of dimensionless pressures calculated from analytical and numerical solutions for transient flow in double-porosity, fractured rock.

Appendix A. Steady-State Solution for Single-Phase Flow

The steady-state flow problem considered here is fluid production from a fully penetrating well in a finite, radial system, subject to a constant outer boundary pressure.

$$\frac{\partial}{\partial r}\left[\rho(P)\, r\, v_r\right] = 0 \tag{A.1}$$

where v_r is volumetric flow rate along the r-direction. At the outer boundary ($r = r_e$),

$$P(r = r_e) = P_i \qquad \text{(constant)} \tag{A.2}$$

and at the inner boundary of the wellbore, $r = r_w$, the fluid is produced at a constant mass rate,

$$2\pi r_w h\left[\rho\, v_r\right]_{r=r_w} = q_m \qquad \text{(constant)} \tag{A.3}$$

Integrating Equation (A.1) leads to

$$\left[\rho(P)\, r\, v_r\right] = C \tag{A.4}$$

and using (A.3), we have

$$\left[\rho(P)\, r\, v_r\right] = \frac{q_m}{2\pi h} \tag{A.5}$$

For the one-dimensional, horizontal, single-phase non-Darcy flow, v_r can be determined from

Equation (2.2) as

$$v_r = \frac{1}{2k\rho\beta}\left\{-\mu + \left[\mu^2 + 4k^2\rho\beta\frac{\partial P}{\partial r}\right]^{1/2}\right\} \tag{A.6}$$

We have

$$\frac{r}{2k\beta}\left\{-\mu + \left[\mu^2 + 4k^2\rho\beta\frac{\partial P}{\partial r}\right]^{1/2}\right\} = \frac{q_m}{2\pi h} \tag{A.7}$$

or

$$4k^2\rho\beta\frac{\partial P}{\partial r} = 2\mu\frac{kq_m\beta}{\pi h}\frac{1}{r} + \left(\frac{kq_m\beta}{\pi h}\frac{1}{r}\right)^2 \tag{A.8}$$

To solve Equation (A.8), we correlate the fluid density as a function of pressure

$$\rho = \rho(P) = \rho_i\left[1 + C_f\left(P - P_i\right)\right] \tag{A.9}$$

$$\left[1 + C_f\left(P - P_i\right)\right]\frac{\partial P}{\partial r} = \frac{q_v\mu}{2\pi kh}\frac{1}{r} + \frac{q_v\mu}{2\pi kh}\frac{kq_m\beta}{2\pi h\mu}\frac{1}{r^2} \tag{A.10}$$

where $q_v = q_m/\rho_i$, is the volumetric production rate at the reference pressure. In terms of dimensionless variables,

$$-\left[1-Q_D P_D\right]\frac{\partial P_D}{\partial r_D}=\frac{1}{r_D}+\beta_D\frac{1}{r_D^2} \tag{A.11}$$

where

$$Q_D=\frac{q_v\mu C_f}{2\pi kh} \tag{A.12}$$

Finally, we have the steady-state solution:

$$P_D=\frac{1-\left[1-2Q_D\left(\ln\left(\frac{r_D^e}{r_D}\right)+\beta_D\left(\frac{1}{r_D}-\frac{1}{r_D^e}\right)\right)\right]^{1/2}}{Q_D} \tag{A.13}$$

where,

$$r_D^e=\frac{r_e}{r_w} \tag{A.14}$$

If we introduce a constant density in Equation (A.8), we arrive at the simple steady-state solution

$$P_D=\ln\left(\frac{r_D^e}{r_D}\right)+\beta_D\left(\frac{1}{r_D}-\frac{1}{r_D^e}\right) \tag{A.15}$$

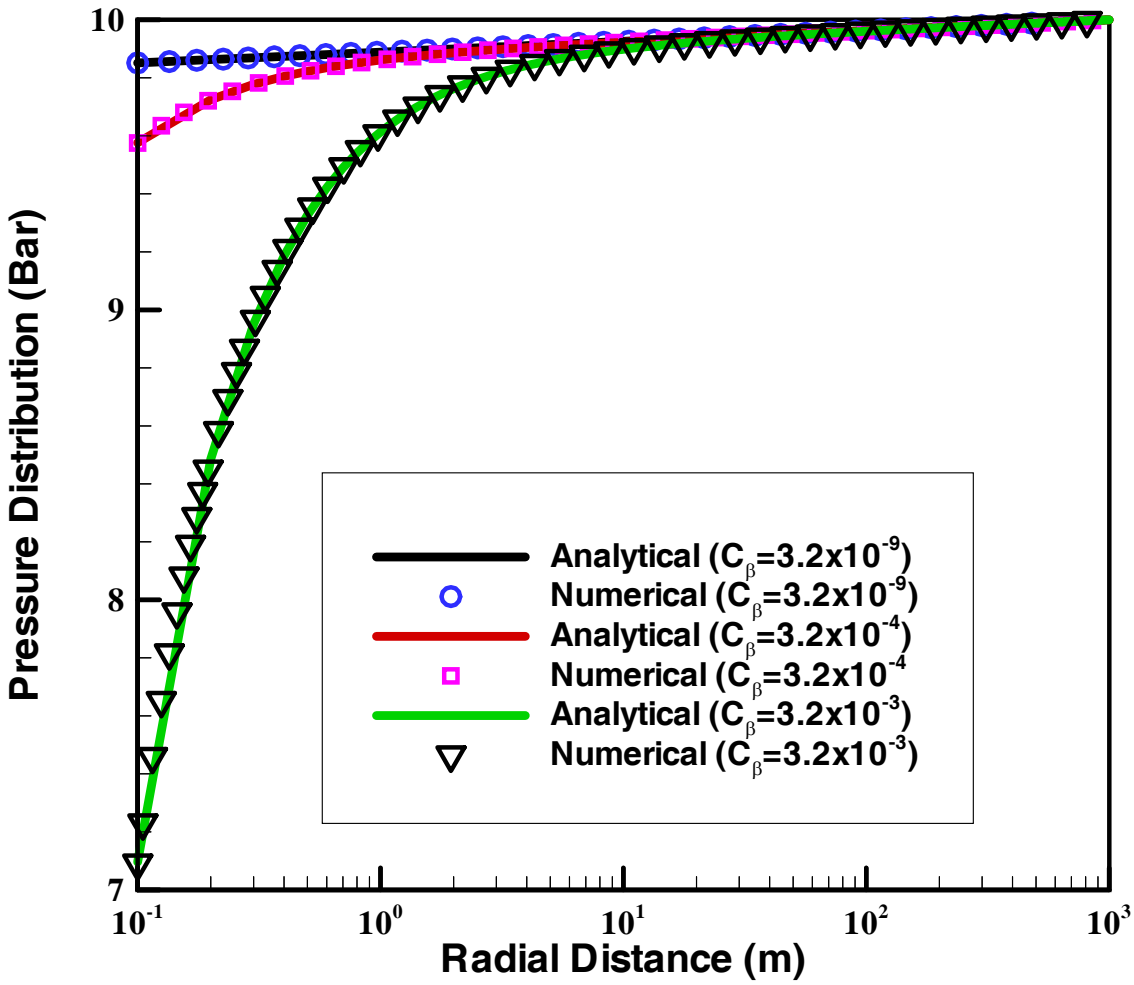

Figure 5.1 Comparison of dimensionless pressures calculated from exact and numerical solutions for steady-state non-Darcy flow with different non-Darcy flow coefficients.

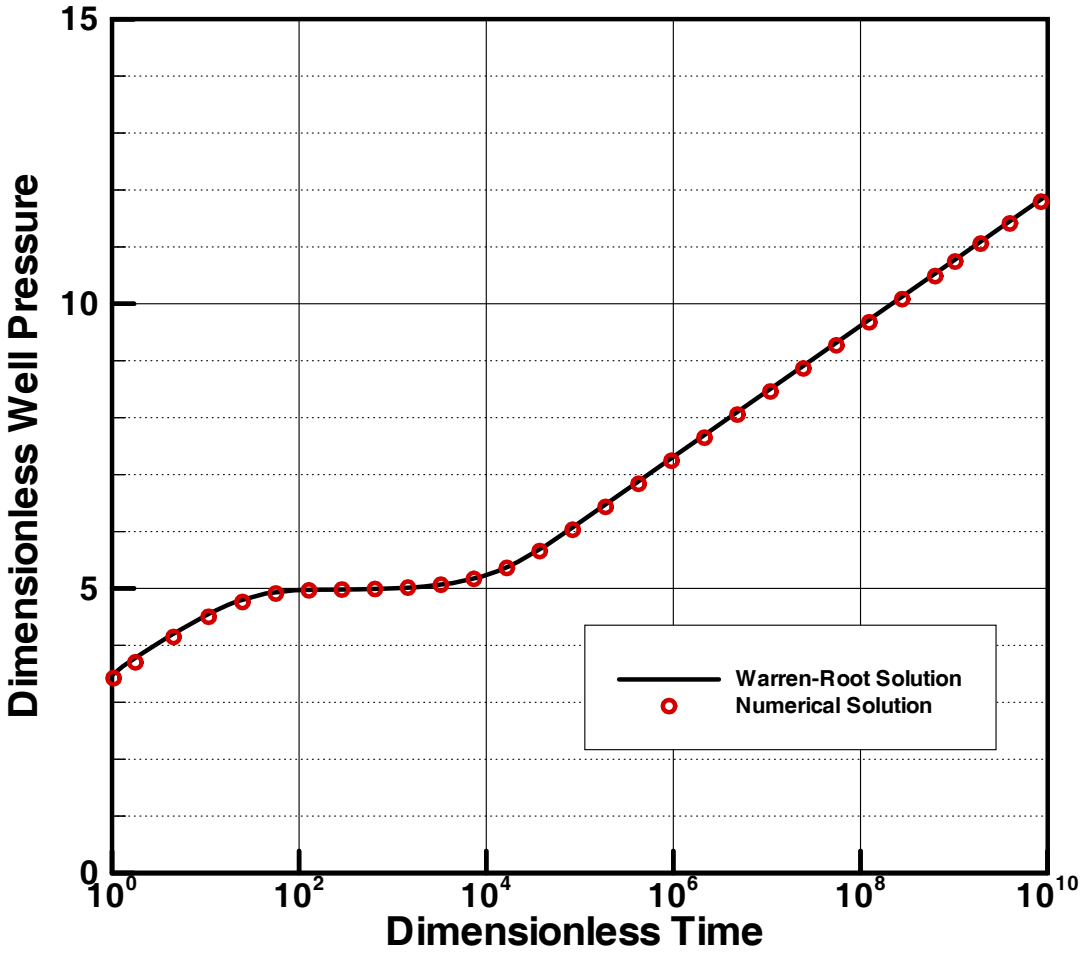

Figure 5.2 Comparison of dimensionless pressures calculated from analytical and numerical solutions for transient flow in double-porosity, fractured rock.

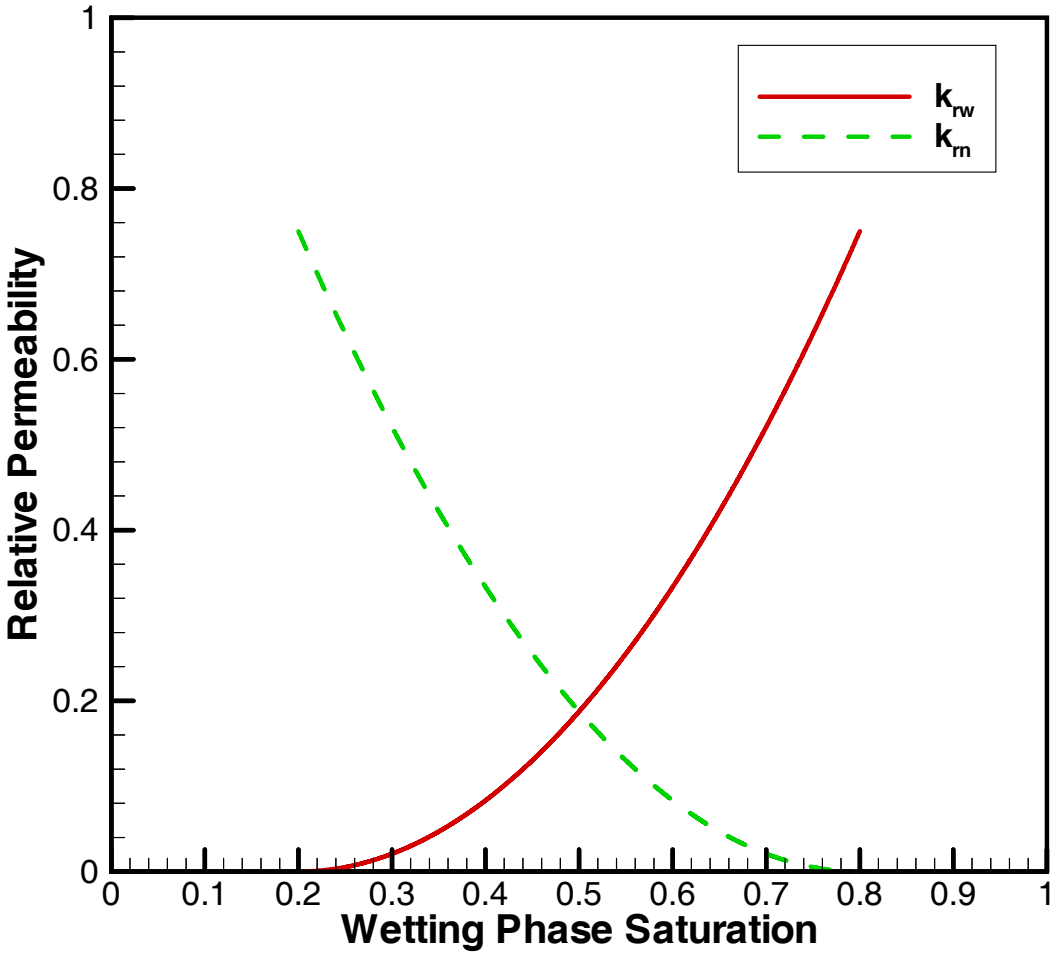

Figure 5.3 Relative-permeability curves used in analytical and numerical solutions for non-Darcy displacement.

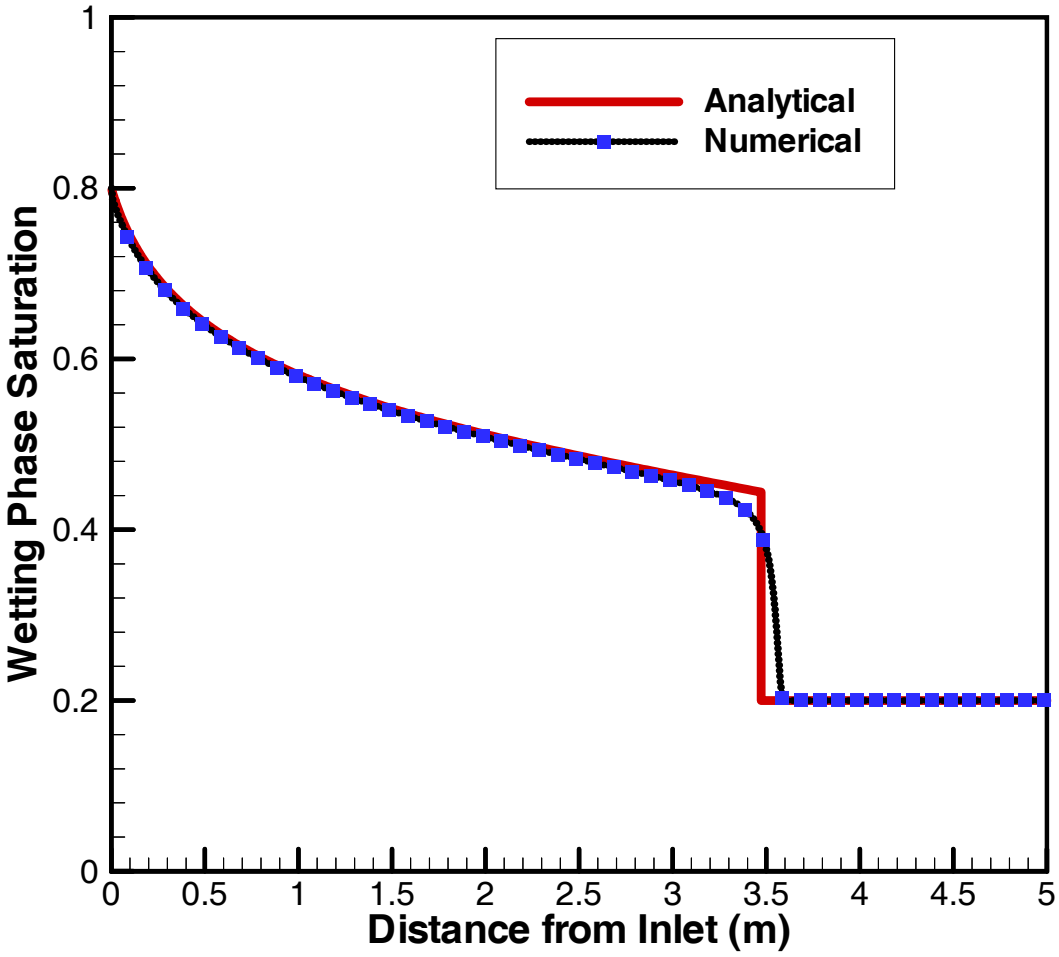

5.4 Comparison between saturation profiles calculated from analytical and numerical solutions after 10 hours of injection.

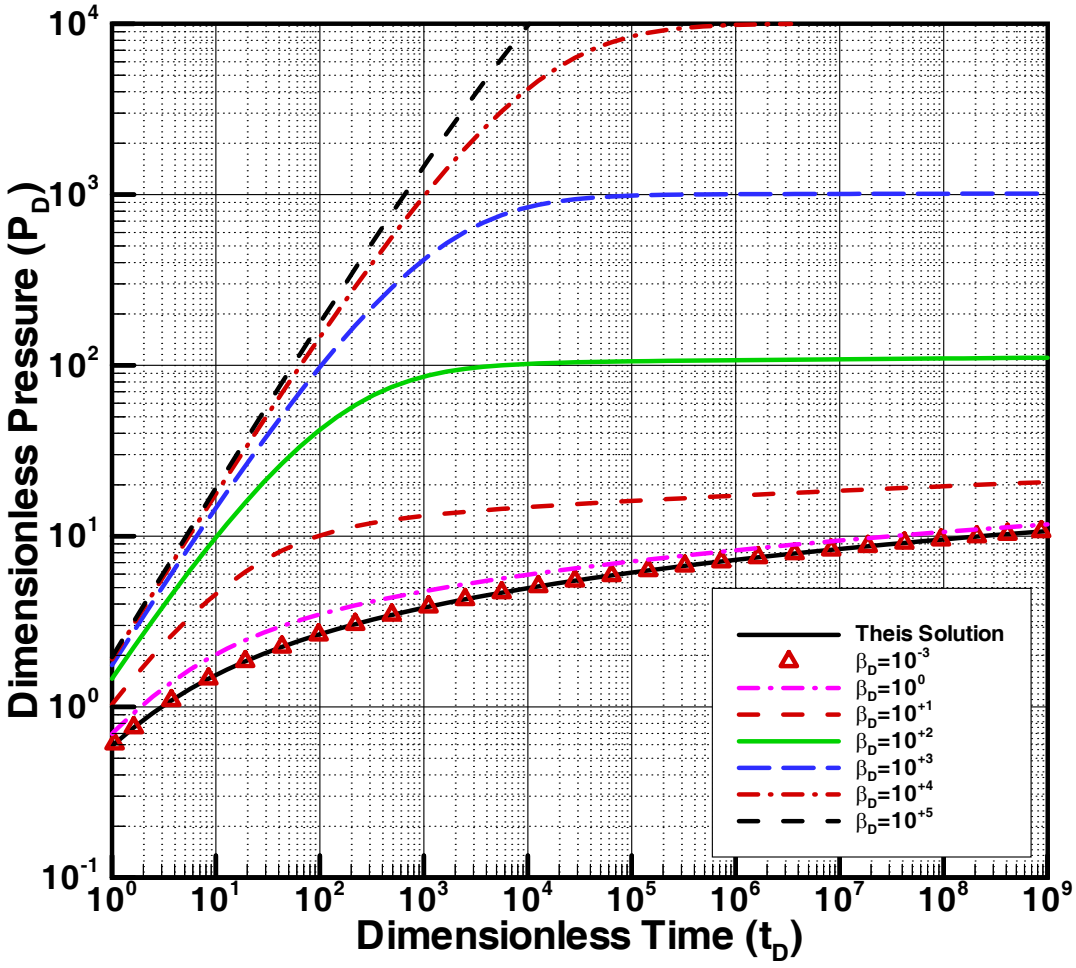

Figure 6.1 Type curves for dimensionless pressures for non-Darcy flow in an infinite system without wellbore storage and skin effects.

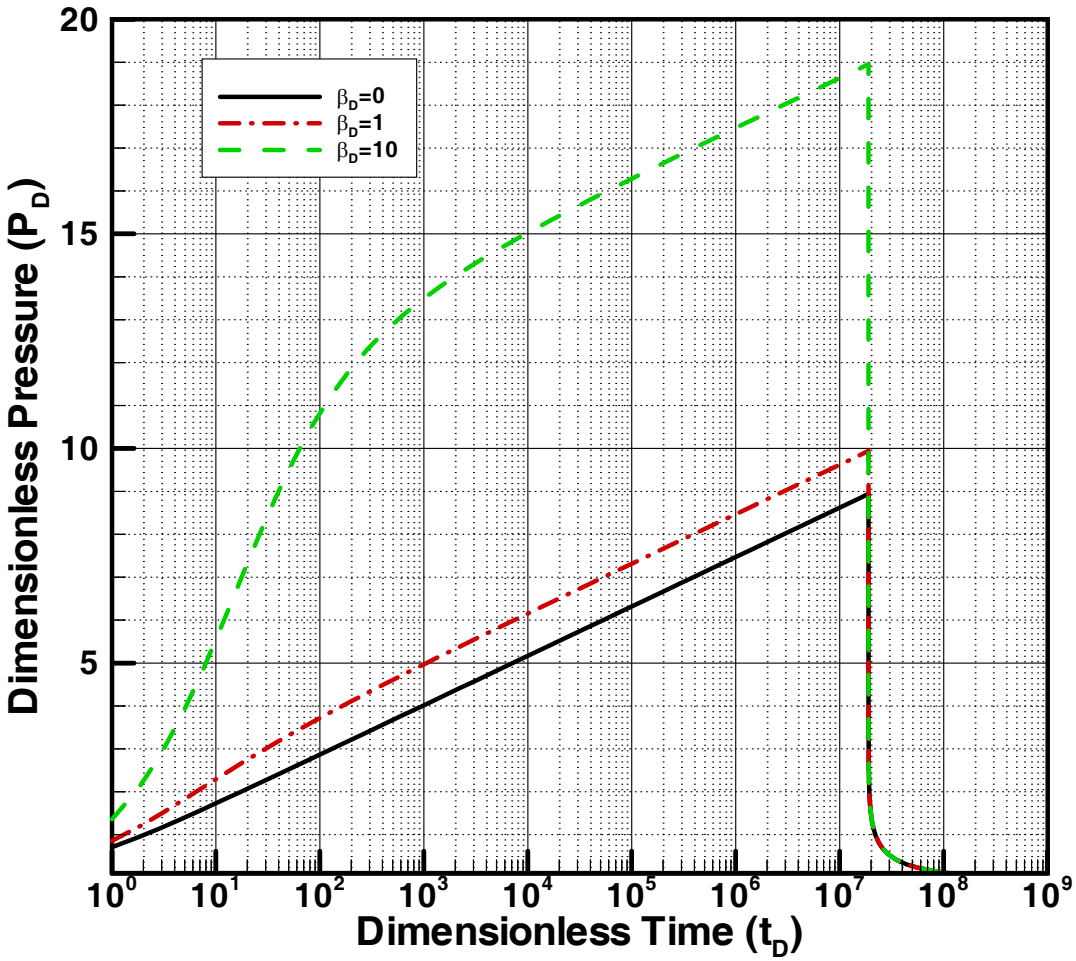

Figure 6.2 Dimensionless pressures for one-day pumping, followed by pressure buildup, of non-Darcy flow in an infinite system without wellbore storage and skin effects.

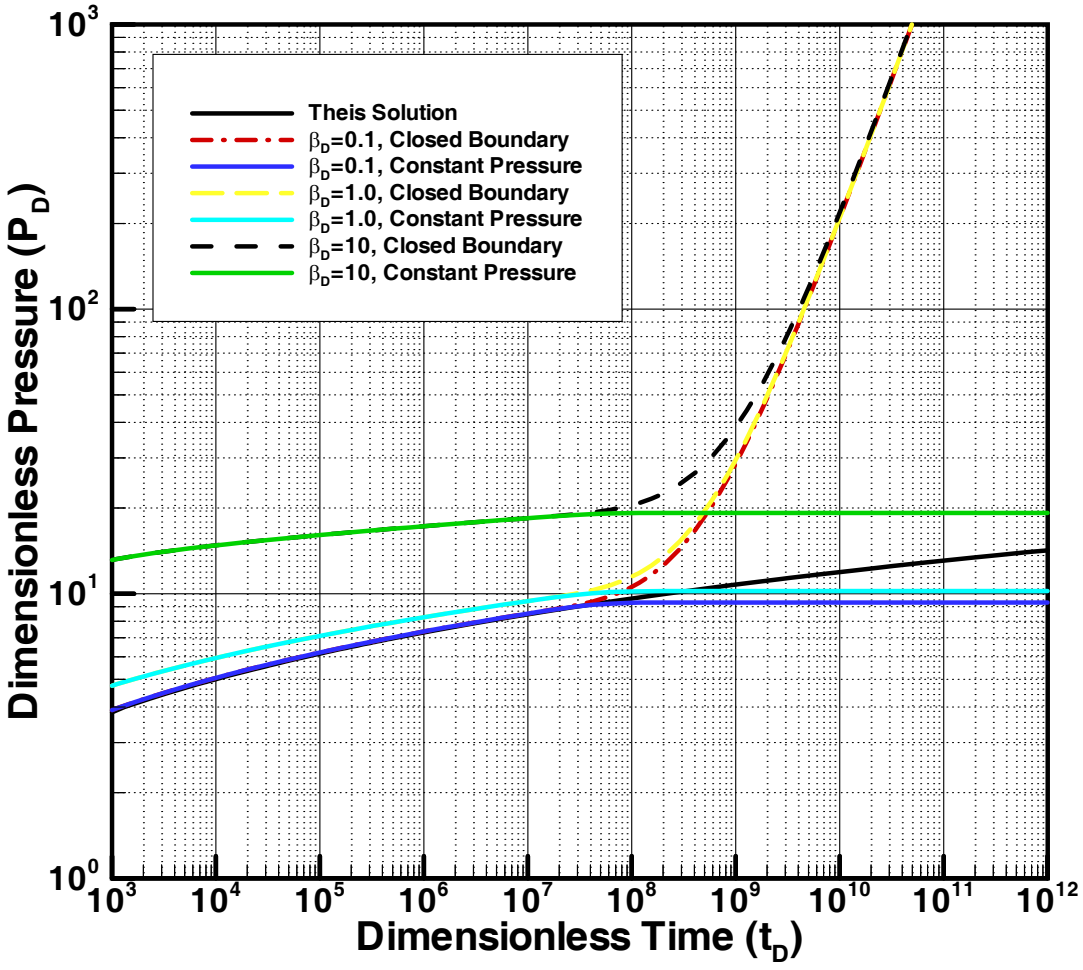

Figure 6.3 Type curves for dimensionless pressures for non-Darcy flow in a finite system with an outer boundary radius of 1,000 m.

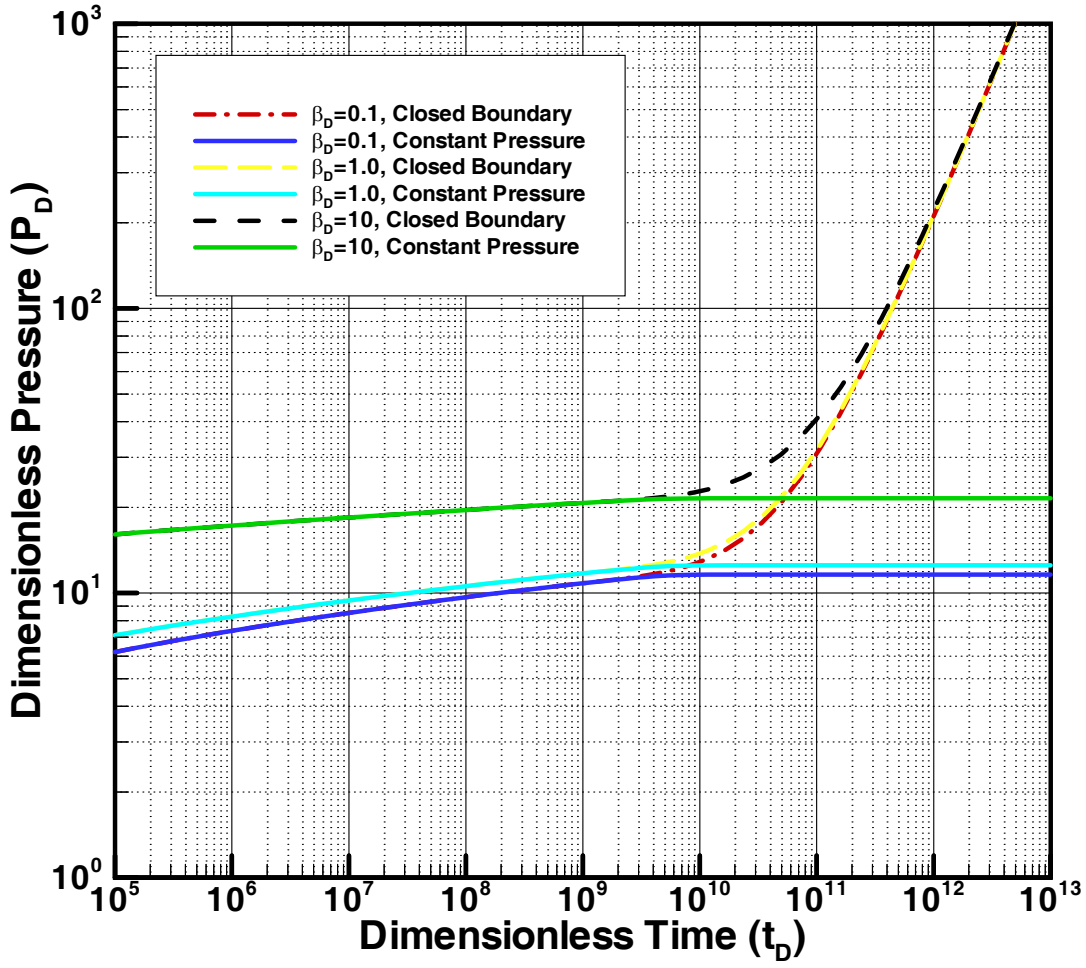

Figure 6.4 Type curves for dimensionless pressures for non-Darcy flow in a finite system with an outer boundary radius of 10,000 m.

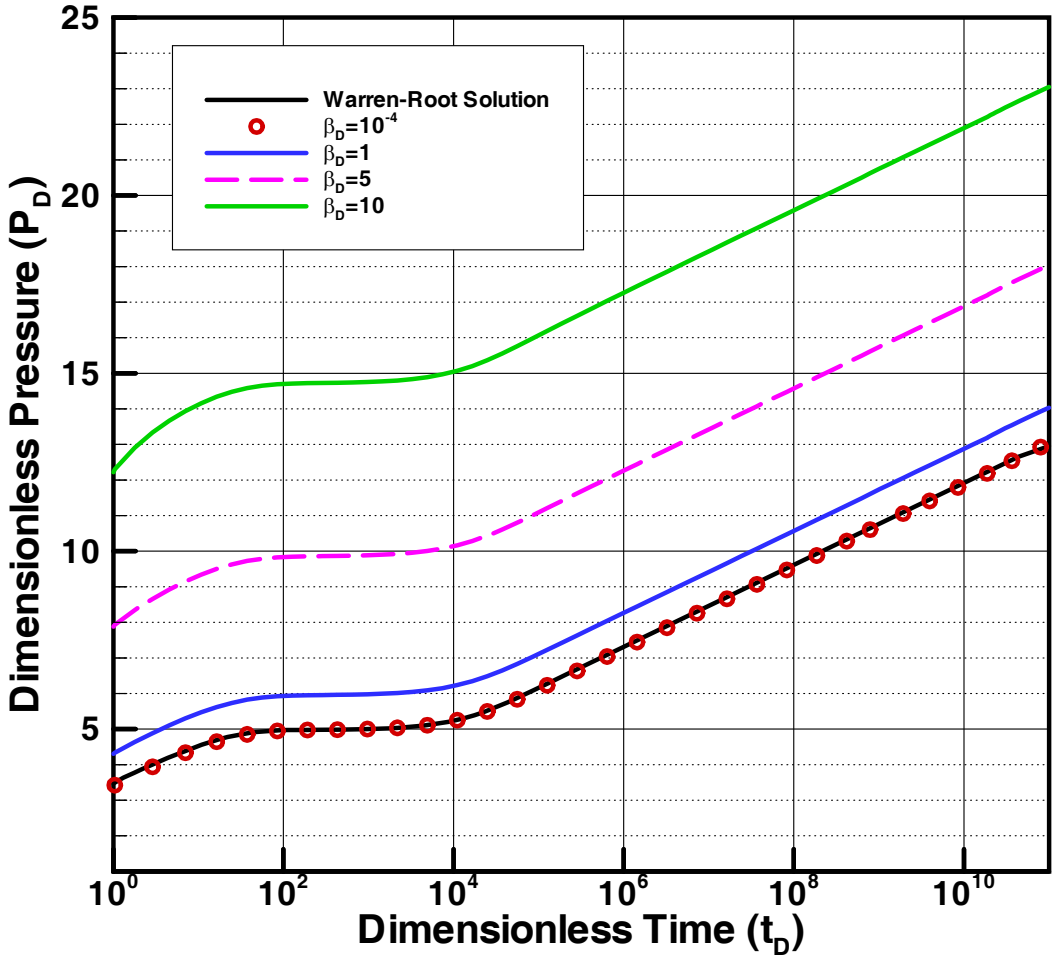

Figure 6.5 Type curves for dimensionless pressures for non-Darcy flow in an infinite fractured system without wellbore storage and skin effects (dimensionless non-Darcy flow coefficients for fracture systems).